doi:10.1093/brain/awz296 BRAIN 2019: 142; 3565–3579 | 3565

BRAIN
A JOURNAL OF NEUROLOGY

Intrastriatal alpha-synuclein fibrils in monkeys: spreading, imaging and neuropathological changes

Yaping Chu,[1] Scott Muller,[1] Adriana Tavares,[2] Olivier Barret,[2] David Alagille,[2] John Seibyl,[2] Gilles Tamagnan,[2] Ken Marek,[2] Kelvin C. Luk,[3,4] John Q. Trojanowski,[3] Virginia M. Y. Lee[3] and Jeffrey H. Kordower[1]

See Dehay and Bezard (doi:10.1093/brain/awz329) for a scientific commentary on this article.

Several studies have demonstrated that intrastriatal injections of fibrillar α-synuclein in rodent brain induced a Parkinson's disease-like propagation of Lewy body pathology with significant nigrostriatal neurodegeneration. This study evaluated the pathological features when exogenous α-synuclein preformed fibrils were injected into the putamen of non-human primates. Eight cynomolgus monkeys received unilateral intraputamen injections of α-synuclein preformed fibrils and four monkeys received sham surgery. Monkeys were assessed with ^{123}I-PE2I single-photon emission computerized tomography scans targeting the dopamine transprter at baseline, 3, 6, 9, 12, and 15 months. Imaging revealed a robust increase in dopamine transporter binding, an effect confirmed by port-mortem immunohistochemical analyses, suggesting that upregulation of dopamine transporter occurs as part of an early pathological process. Histochemistry and immunohistochemistry revealed that α-synuclein preformed fibrils injections into the putamen induced intraneuronal inclusions positive for phosphorylated α-synuclein in ipsilateral substantia nigra and adjacent to the injection site. α-Synuclein inclusions were thioflavin-S-positive suggesting that the inclusions induced by α-synuclein preformed fibrils exhibited pathological properties similar to amyloid-like Lewy body pathology in Parkinson's disease brains. The α-synuclein preformed fibrils resulted in Lewy pathology in the ipsilateral substantia nigra with significant reduction (−29.30%) of dopaminergic neurons as compared with controls. Nigral neurons with α-synuclein inclusions exhibited a phenotypic downregulation of the dopamine markers tyrosine hydroxylase and Nurr1. Taken together, our findings demonstrate that α-synuclein preformed fibrils induce a synucleinopathy in non-human primates with authentic Lewy pathology and nigrostriatal changes indicative of early Parkinson's disease.

1 Department of Neurological Sciences, Rush University Medical Center, Chicago, IL 60612, USA
2 Molecular NeuroImaging, LLC New Haven 06510, CT, USA
3 Department of Pathology and Laboratory Medicine, University of Pennsylvania School of Medicine, Philadelphia 19104, PA, USA
4 Center for Neurodegenerative Disease Research, University of Pennsylvania School of Medicine, Philadelphia 19104, PA, USA

Correspondence to: Jeffrey H. Kordower, PhD
Department of Neurological Sciences
Rush University Medical Center
1735 West Harrison Street
Chicago, Illinois 60612, USA
E-mail: Jeffrey_Kordower@rush.edu

Keywords: α-synuclein; Lewy bodies; propagation; nigrostriatal system; neurodegeneration

Abbreviations: DAT = dopamine transporter; PFF = preformed fibrils; SPECT = single-photon emission computerized tomography; SUVR = standardized uptake value ratio

Received April 24, 2019. Revised July 17, 2019. Accepted August 1, 2019. Advance Access publication October 3, 2019

Introduction

α-Synuclein (α-syn) inclusions have been observed in foetal grafts implanted into Parkinson's disease patients brains more than a decade prior (Kordower *et al.*, 2008, 2017; Li *et al.*, 2008; Chu and Kordower, 2010). These findings lead to the provocative hypothesis that α-syn is a pathogenic agent that can propagate from diseased neurons within their connectome by permissive templating, thereby spreading pathology in the brain of Parkinson's disease and other α-synucleinopathies (Kordower and Brundin, 2009; Steiner *et al.*, 2011; Luk *et al.*, 2012; Chu and Kordower, 2015). Indeed, when α-syn preformed fibrils (PFFs) were added to primary neurons from α-syn knockout mice (Volpicelli-Daley *et al.*, 2011) or injected into the striatum of α-syn knockout mice (Luk *et al.*, 2012), phosphorylated α-syn and cell death were not detected (Volpicelli-Daley *et al.*, 2014) supporting the concept that the spreading process involves permissive templating.

Misfolded α-syn is an integral pathology in a variety of neurodegenerative disorders including Parkinson's disease. Several observations demonstrate that α-syn PFFs (Volpicelli-Daley *et al.*, 2011; Luk *et al.*, 2016; Froula *et al.*, 2018) or Lewy body extracts (Recasens and Dehay, 2014) convert normal α-syn to pathological α-syn via permissive templating thus spreading Parkinson's disease pathology throughout the brain. Towards this end, α-syn PFFs synthesized from recombinant α-syn and seeded in mouse or rat striatum can propagate to different brain areas and recruit endogenous α-syn into aggregates characterized by detergent-insolubility and hyperphosphorylation (Luk *et al.*, 2012; Paumier *et al.*, 2015). A combination of adeno-associated virus-mediated overexpression of α-syn and α-syn PFFs injected into rat brains induced acute and rapid dopamine neurodegeneration and inflammatory reactions (Thakur *et al.*, 2017). Interestingly, Lewy body extracts from Parkinson's disease brain, delivered into the substantia nigra or striatum of macaque monkeys, triggered intracellular and presynaptic α-syn accumulations and nigrostriatal neurodegeneration (Recasens *et al.*, 2014). These studies have repeatedly verified that exogenous α-syn PFFs or Lewy body extracts are the initiator and the endogenous α-syn is an essential donor for forming Parkinson-like pathology and neurodegeneration in rodents. Given the complexity of human neuroanatomy and physiology, however, models more phylogenetically similar to humans are needed. Indeed, although rodents remain the most widely used order for animal models of Parkinson's disease, they display little or modest age-related changes in nigrostriatal dopamine (Irwin *et al.*, 1992; Pasinetti *et al.*, 1992; Dawson *et al.*, 2002) and do not display age-related loss of tyrosine hydroxylase (TH) immunoreactivity in nigral cells (McNeill and Koek, 1990). Our previous studies demonstrated that non-human primates displayed age-associated increase of α-syn (Chu and Kordower, 2007), loss of TH (Kanaan *et al.*, 2007), and age-relative diminished compensation in the nigrostriatal system (Collier *et al.*, 2007) similar to what is seen in humans. To further determine whether α-syn PFFs induce parkinsonian-like pathology, we used non-human primates to examine the pathological alterations of dopaminergic neurons in vivo with serial dopamine transporter (DAT) single-photon emission computerized tomography (SPECT) scans and in brain tissue with histochemistry and immunohistochemistry.

Materials and methods

Injection of α-synuclein preformed fibrils

Twelve cynomolgus monkeys ranging 6 to 10 years of age were used in this study. Eight animals received three injections of α-syn PFFs (2 mg/ml) into right putamen (10 µl, 10 µl, 5 µl) and four received sham surgery (Table 1). Coordinates for stereotaxic injection were based upon MRI guidance. Prior to surgery, monkeys were anaesthetized with an intramuscular injection of ketamine (3 mg/kg) and dexmedetomidine (0.03 mg/kg). Once in an anaesthetic plane, the monkeys were placed in a specially designed MRI compatible stereotaxic frame modelled after a Kopf primate stereotaxic frame. The angle of the head was established by measuring the height of an incisor tooth using a standard micromanipulator and a modified electrode holder. Then the monkey was transferred to a 3.0 T MRI unit (GE Healthcare). Coronal T_1-weighted images were acquired at a 2-mm slice thickness with 1 mm interpolation. The coordinates for injection were measured separately for each animal using the MRI unit's built-in software. The most rostral injection was targeted to the putamen at the level of the optic chiasm (roughly 15.0 mm anterior to the interaural line, 10.1 mm lateral to the midsagittal plane, and 18.1 mm ventral to dura) before the decussation of the anterior commissure. The second injection was targeted to the

Table 1 Stereological analysis of p-S129-α-syn-immunoreactive cells in substantia nigra

Case	Injection of α-synuclein PFFs	Number of p-S129-α-syn-immunoreactive cells
CN8172	Yes	1084
CN8408	Yes	1251
CN8409	Yes	853
CN8410	Yes	2868
CN8411	Yes	8010
CN8413	Yes	4132
CN8414	Yes	3194
CN8415[a]	Yes	0
CN8582	No	0
CN8622	No	0
CN8624	No	0
CN8623	No	0

[a]Died at 3 months after surgery.

putamen at the level of decussation of the anterior commissure (roughly 12.0 mm anterior to the interaural line, 10.4 mm lateral to the midsagittal plane, and 18.4 mm ventral to dura). The most caudal injection was targeted to the putamen at the level of the anterior hippocampus caudal to the decussation of the anterior commissure (roughly 9.0 mm anterior to the interaural line, 13.1 mm lateral to the midsagittal plane, and 17.6 mm ventral to dura). Monkeys were housed one per cage on a 12-h on/12-h off lighting cycle with *ad libitum* access to food and water. The quality of the animal care exceeded the recommended NIH guidelines. Institutional Animal Care and Use Committee at Rush University Medical Center approved this study (Rush IACUC#12-067).

^{123}I-PE2I synthesis and SPECT image acquisition

High specific activity ^{123}I-PE2I was synthesized as previously described (Chang *et al.*, 2013). ^{123}I-MNI-420 was prepared as described previously (Tavares *et al.*, 2013). The specific activity of the radiotracer was higher than 200 Ci/μmol and the radiochemical purity was >90%. Approximately 4–5 mCi of ^{123}I-PE2I was injected intravenously. SPECT studies were acquired on a MollyQ SPECT device (Neurophysics Corp.). These cameras use an array of 12 scanning heads with focused collimation, collecting photons into a symmetric energy window centred at 159 kEv (±10%). The unique geometry of these instruments provides ultra-high resolution images with an in-plane and in *z*-axis full-width at half-maximum of 4.5 mm. An intravenous line was placed and used for injection of the ^{123}I-PE2I. Following injection of ^{123}I-PE2I a series of 11–15 dynamic SPECT scans were obtained as serial 15–20-min acquisitions continuously over the duration of the study (~4 h), with the animals remaining in the camera for the whole study. PE2I (DAT) SPECT Scans were performed at baseline, 3, 6, 9, 12, and 15 months.

Image analysis

The raw imaging data were provided to Molecular NeuroImaging where they were reconstructed, and filtered using a standardized 3D algorithm provided by the camera manufacturer. Reconstructed image data volumes were transferred to the image processing PMOD software (PMOD Technologies, Zurich, Switzerland) where the images were merged to create a dynamic series, radioactive decay corrected, and motion corrected. All images were corrected for attenuation using the Chang method (Chang *et al.*, 2013) with ellipses manually drawn on the baseline image (linear attenuation coefficient $\mu = 0.11\ cm^{-1}$). A calibration factor of 2.27 was applied to the images to convert them to units of kBq/cm^3. Dynamic images were realigned and co-registered to a common orientation defined by an MRI cynomolgus primate brain template. Volumes of interest were manually defined and drawn in the common template space on the left and right striatum (DAT rich), and on the occipital cortex, representing the non-specific binding. Average activity concentration (kBq/cm^3) within each volume of interest was determined and time-activity curves were generated for each study, depicting the regional brain activity concentration over time. Time-activity curves were expressed in standardized uptake value units (g/ml) by normalizing by the weight of the animal and the injected activity. The striatal time-activity curves were divided by the occipital cortex time-activity curve to generate standardized uptake value ratio (SUVR) curves. The binding in the striatum was quantified using the total (specific + non-specific) to non-specific signal ratios calculated by averaging the SUVR curves at late times (~150–240 min), during which ^{123}I-PE2I was at steady state (i.e. SUVR curves reached a plateau).

Tissue acquisition

Monkeys were sacrificed at 12–15 months after surgery for histochemical analysis. Monkeys were pretreated with ketamine (20 mg/kg, intramuscularly) and then were deeply anaesthetized with sodium pentobarbital (25 mg/kg, intravenously). Prior to perfusion, monkeys were injected with 1 ml of heparin (20 000 IU) into the left ventricle of the heart. Animals were then perfused through the ascending aorta with physiological saline, followed by 1 l of 4% ice-cold paraformaldehyde. The brains were then removed from the calvaria, post-fixed in the same fixative solution overnight, progressively transferred through 10%, 20%, and 30% sucrose, and sectioned on a freezing microtome at 40 μm in the coronal plane. All sections were collected and stored in order in a cryoprotectant solution (30% sucrose and 30% ethylene glycol in 0.1 M phosphate-buffered saline, pH 7.4) before processing.

Immunohistochemical and histochemical procedures

An immunoperoxidase labelling method was used to visualize phosphorylated α-syn, DAT, and TH. The rabbit monoclonal α-syn (p-S129-α-syn) antibody (Abcam, ab51253) selectively detects α-syn phosphorylated on Ser129 (Chu *et al.*, 2012; Kellie *et al.*, 2014). The monoclonal DAT antibody (Millipore, MAB369) detects the N-terminus of DAT and primarily labels presynaptic dopaminergic nerve terminals (Miller *et al.*, 1997). The monoclonal TH antibody (ImmunoStar, 22941) recognizes a conserved epitope in catalytic core of the TH enzyme (Wiemerslage *et al.*, 2013). One series of sections for each antibody was immunostained with p-S129-α-syn antibody (1:500), DAT (1:5000), and TH (1:10,000) overnight at room temperature. After six washes, sections were incubated for 1 h in biotinylated goat anti-rabbit IgG (1:200; Vector) for p-S129-α-syn, goat anti-rat (1:200; Vector) for DAT, and horse anti-mouse (1:200; Vector) for TH followed by the Elite avidin–biotin complex (1:500, ABC kits; Vector). The immunohistochemical reaction was completed with 0.05% DAB and 0.005% H_2O_2. Sections were mounted on gelatin-coated slides, dehydrated through graded alcohol, cleared in xylene, and coverslipped with Cytoseal^{TM}. Thioflavin S histochemistry was performed to determine whether p-S129-α-syn antibody-labelled inclusions contained amyloid fibrils with beta pleated sheet structures analogous to Lewy pathology in human synucleinopathies. Midbrain sections were mounted on gelatin-coated slides and dried at room temperature. Mounted sections were defatted in equal parts of chloroform and 100% ethanol for 2 h and stained with 0.1% thioflavin S for 10 min in

the dark (Kordower *et al.*, 2008). The stained inclusions were visualized with fluorescent microscopy.

Stereological quantification of p-S129-α-syn and TH immunoreactive cell number

To estimate the number of nigral neurons with α-syn inclusions and the number of TH immunopositive neurons, an optical fractionator unbiased sampling design was used to estimate the total number of p-S129-α-syn or TH labelling cells within the substantia nigra (Chu *et al*, 2012; Gundersen *et al.*, 1988). We evaluated the whole substantia nigra in each animal. The section sampling fraction (ssf) was 1/0.042. The distance between sections was ~0.96 mm. In cross-section, the substantia nigra is located in the ventral midbrain. The substantia nigra pars compacta was outlined using a 1.25× objective. A systematic sample of the area occupied by the substantia nigra pars compacta was made from a random starting point (StereoInvestigator v2018.1.1 software; MicroBrightField, Colchester, VT). Counts were made at regular predetermined intervals (x = 313 μm, y = 313 μm), and a counting frame (70 × 70 μm = 4900 μm^2) was superimposed on images obtained from tissue sections. The area sampling fraction (asf) was 1/0.2. These sections were then analysed using a 60× Planapo oil immersion objective with a 1.4 numerical aperture. The section thickness was empirically determined. Briefly, as the top of the section was first brought into focus, the stage was zeroed at the z-axis by software. The stage then stepped through the z-axis until the bottom of the section was in focus. Section thickness averaged 16.21 ± 2.3 μm in the midbrain. The disector height (counting frame thickness) was 10 μm. This method allowed for 2 μm top guard zones and at least 2 μm bottom guard zones. The thickness sampling fraction (tsf) was 1/0.61. Care was taken to ensure that the top and bottom forbidden planes were never included in the cell counting. Using stereological principles, p-S129-α-syn- or TH-immunoreactive neurons in each case were sampled using a uniform, systematic, and random design. The total number of p-S129-α-syn- or TH-immunoreactive neurons within the substantia nigra was calculated separately using the following formula:

$$n = \Sigma Q - \cdot 1/ssf \cdot 1/asf \cdot 1/tsf \quad (1)$$

where ΣQ was the total number of raw counts. The coefficients of error (CE) were calculated according to the procedure of Gunderson and colleagues as estimates of precision (Schmitz and Hof, 2000). The values of CE were 0.14 ± 0.05 (range 0.10 to 0.19) for p-S129-α-syn-immunoreactive neuronal counts and 0.10 ± 0.02 (range 0.08 to 0.12) for TH-immunoreactive neuronal counts.

Immunofluorescence double-labelling

A double-label immunofluorescence procedure was used to determine whether TH and Nurr1 expression was effected by α-syn accumulation. Sections through the substantia nigra from each brain were incubated in the mouse primary antibodies TH (1:5000) and Nurr1 (1:250; monoclonal antibody; Abcam; ab4117) overnight at room temperature and the goat anti-mouse antibody coupled to Alexa Fluor® 647 (1:200; Jackson ImmunoResearch) for 1 h. After six washes in Tris-buffered saline pH 7.4 (TBS), the sections were blocked again for 1 h in a solution containing 5% goat serum, 2% bovine serum albumin, and 0.3% Triton™ X-100 in TBS. Sections were then incubated in the second primary p-S129-α-syn rabbit monoclonal antibody (1:500) overnight and the goat anti-rabbit antibody coupled to DyLight™ 488(1:200) for 1 h. The co-localization of p-S129-α-syn/DAT or p-S129-α-syn/DARPP-32 in putamen was examined with fluorescence double-labelling methods. The sections were mounted on gelatin-coated slides and allowed to air dry overnight, dehydrated through graded alcohol, cleared in xylene, and coverslipped with DPX.

Fluorescence intensity measurements

The measurements were performed according to our previously published procedures (Chu *et al.*, 2012, 2014). All immunofluorescence double-labelled images were scanned with an Olympus Confocal Fluoroview Microscope equipped with argon and helium-neon lasers. With a 20× magnification objective and a 488 and 633 nm excitation source, images were acquired at each sampling site in the substantia nigra or putamen and were saved to a Fluoroview file. Following acquisition of an image, the stage moves to the next sampling site to ensure a completely non-redundant evaluation. Once all images were acquired, optical density measurements were performed on individual neurons. To maintain consistency of the scanned image for each slide, the laser intensity, confocal aperture, photomultiplier voltage, offset, electronic gain, scan speed, image size, filter and zoom were set for the background level whereby autofluorescence was not visible with a control section. These settings were maintained throughout the entire experiment (Chu *et al.*, 2014). The intensity mapping sliders ranged from 0 to 4095; 0 represented a maximum black image and 4095 represented a maximum bright image. The TH-immunoreactive neurons with or without p-S129-α-syn-immunoreactive inclusions were identified and outlined separately. Quantitative optical density of immunofluorescence was performed on individual TH- and DARPP-32-immunoreactive perikarya or Nurr1-immunoreactive nuclei with or without α-syn-immunoreactive inclusions in different channels. For TH and Nurr1, five equispaced sections across the entire length of the substantia nigra were sampled and evaluated. For DARPP-32, the sections with PFFs injections were sampled and evaluated. To account for differences in background staining intensity, five background intensity measurements lacking immunofluorescent profiles were taken from each section. The mean of these five measurements constituted the background intensity that was then subtracted from the measured optical density of each individual neuron to provide a final optical density value. To confirm co-localization of the double labelling, optical scanning through the neuron's z-axis was performed at 1-μm thickness and neurons suspected of being double-labelled were confirmed with confocal cross-sectional analyses.

Optical density measurements of DAT immunoreactivity in the striatum

Quantification of the relative optical density of striatal DAT immunoreactivity was performed using a densitometry software program (ImageJ 1.63; NIH, Bethesda, MD), as described previously (Chu *et al.*, 2012). The DAT-immunostained striatum was outlined manually, and optical density measurements were performed in greyscale (0 represented a maximum bright image and 255 represented a maximum dark image). For each subject, approximately nine equally-spaced sections through the entire striatum were sampled and evaluated. To account for differences in background staining intensity, background optical density measurements in each section were taken from corpus callosum that lacked DAT immunoreactive profile. The mean of these measurements constituted the background optical density that was subtracted from the optical density of DAT immunoreactive intensity measurements to provide a final optical density value. The optical density of TH immunoreactivity in the striatum was measured using same method. Previous studies have shown that optical density measurements reflect changes in protein expression parallel to those obtained using a biochemical protein assay such as western blot (Moeller and Dimitrijevich, 2004).

Data analyses

SUVRs from 3, 6, 9, and 12 month datapoints were compared with baseline and optical density measurements in nigral neurons were compared across groups with repeated measures ANOVA followed by Turkey's multiple comparison test (Prism 4, GraphPad Software, Inc.). Putamenal DAT- and TH-immunoreactive intensities in monkeys that received PFFs were compared with controls using unpaired *t*-test with Welch's correction. The level of significance was set at 0.05 (two-tailed).

Data availability

The data that support the findings of this study are available from the corresponding author, upon reasonable request.

Results

Alterations in PE2I binding by SPECT

SUVR in the left and right striatum at baseline, and at 3, 6, 9, 12, and 15 month datapoints are displayed in Fig. 1 and Supplementary Table 1. A gradual increasing SUVR up to 12 months followed by a plateau or a slightly decreasing binding at the 15-month time points was observed across all monkeys receiving PFFs. The SUVR was remarkably increased about 50% at 9 months and 70% at 12 months from baseline with individual animals demonstrating increases of over 100% relative to baseline (Table 2). Monkeys receiving sham surgery displayed a slightly decreasing binding. A factorial ANOVA revealed a significant difference of SUVR at different time point [$F(4,39) = 10.09$; $P < 0.0001$ in left striatal DAT binding; $F(4,39) = 7.25$; $P < 0.0001$ in right striatal DAT binding]. *Post hoc* analyses revealed a significant increase in binding at 9–12 months in left striatum and right striatum relative to baseline (Table 2). The SUVR results suggested that DAT expression was persistently increased after PFFs were delivered into putamen.

Alterations of DAT and TH immunoreactivities in striatum

To support the imaging data, we stained the striatum for DAT in monkeys receiving the PFFs and sham surgery (control). In control animals DAT staining was light and homogenous (Fig. 2A and B). The staining pattern was similar but with greater staining intensity in monkeys that were injected with PFFs (Fig. 2C and D). Increase DAT-immunoreactivity, similar to that seen with imaging, was bilateral and encompassed the caudate nucleus and putamen. Quantitative optical density measurements (Fig. 2E) demonstrated that DAT staining intensity was higher 16–22% in striatum of monkeys receiving the PFFs than sham surgery. Unpaired *t*-test revealed a statistical significant difference in the optical densities of DAT immunostaining intensities in monkeys with PFFs delivery relative to sham surgery ($t = 6.69$, df = 5, $P = 0.0011$ in caudate nucleus; $t = 5.07$, df = 2, $P = 0.036$ in putamen) supporting the increase of PE2I binding observed in serial SPECT scans. Fluorescence double-labelling revealed that around the PFFs injection site, p-S129-α-syn and DAT was co-localized (Supplementary Fig. 1). The double-labelled structures presented as dots and resembled synapses and small fibres (Supplementary Fig. 1E and F). The coexistence of p-S129-α-syn and DAT was also detected in Parkinson's disease putamen (Supplementary Fig. 1H and I). These data suggested that DAT binds α-syn in Parkinson's disease pathology.

We wanted to determine whether striatal TH expression is also altered following the injection of PFFs. To this end, one series of TH-immunostained striatal sections was analysed. The staining pattern was similar between monkeys received PFFs and sham surgery (Supplementary Fig. 2). TH staining was slightly more intense in monkeys injected with PFFs than in those that received sham surgery. Quantitative analyses further demonstrated that the optical density of TH staining was greater by 8–15% in striatum of monkeys with PFFs than sham surgery, but there was no significant difference between two groups of monkeys (Supplementary Fig, 2E; $t = 2.08$, df = 7, $P = 0.078$ in caudate nucleus; $t = 2.06$, df = 9, $P = 0.068$ or in the putamen).

Distribution and morphological features of p-S129-α-syn-immunopositive inclusions

Immunohistochemistry revealed that p-S129-α-syn-immunoreactive cells were detected in ipsilateral but not in

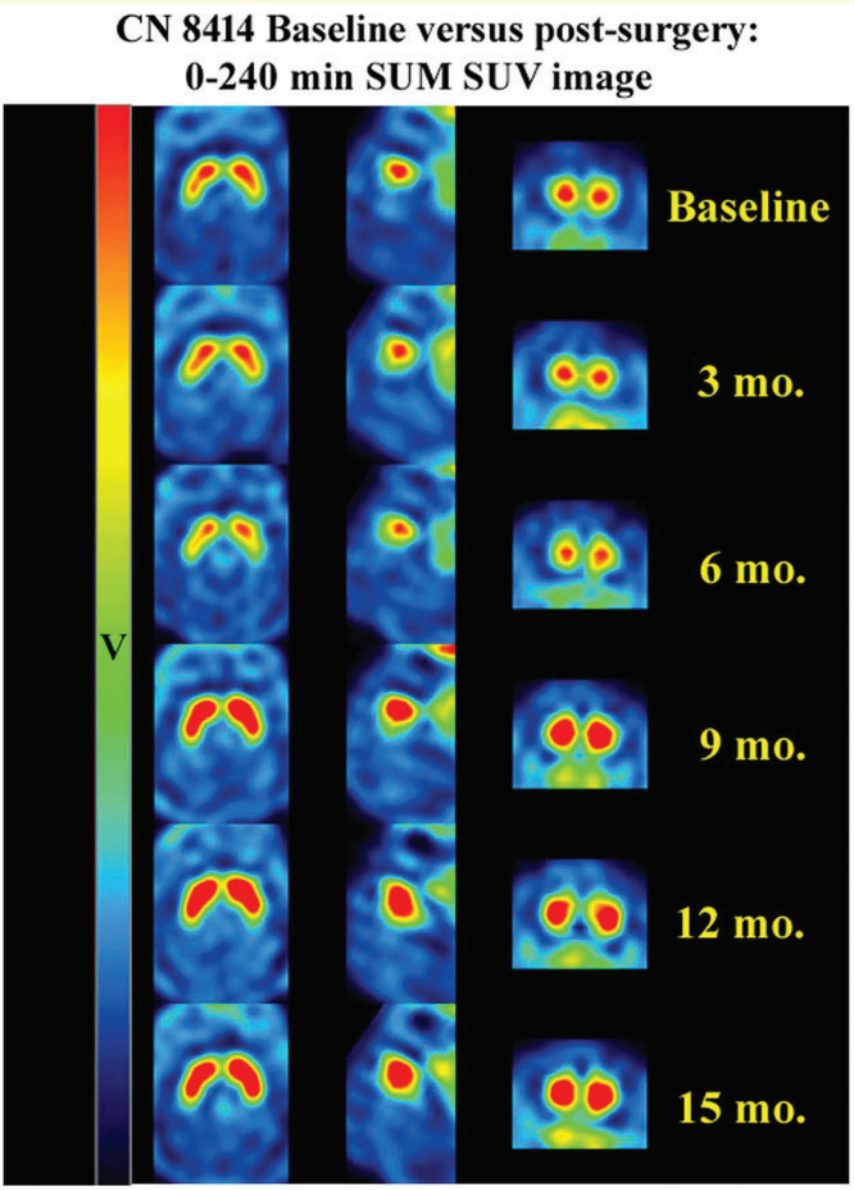

Figure 1 Axial, sagittal, and coronal views of PE2I SPECT scans. There were initial decreases in binding followed by consistent increases in binding for the full 15 months (mo) of scans. v = standardized uptake value.

contralateral putamen and midbrain. In the putamen, strong p-S129-α-syn-immunoreactive cells were observed around the injected area (Fig. 3A) even at the last post-injection time point. The p-S129-α-syn-immunoreactive products were distributed to perikarya and process (Fig. 3B). In putamenal regions, far from injected area, fragmental varicosity p-S129-α-syn-immunoreactive fibres were scattered throughout, but not caudate nuclei (Fig. 3C), suggesting that the segmental p-S129-α-syn-immunoreactive fibres are degenerating axons.

In midbrain the p-S129-α-syn-immunoreactive cells were mainly distributed in ipsilateral substantia nigra pars compacta (Fig. 4B and C). Morphological analyses revealed that there were different shapes and intensities of p-S129-α-syn-immunoreactive cells. Some cells had p-S129-α-syn-immunoreactive granule-like seeds which were distributed within nigral perikarya (Fig. 4D and E). Larger α-syn granules were associated with more cytoplasmic α-syn surrounding them in the perikarya (Fig. 4E and F). When aggregation progresses, the cytoplasmic α-syn is reduced (Fig. 4G). Finally, when the α-syn aggregation became excessive, the monomeric synuclein disappeared, and the aggregate appeared as a round shape similar to a Lewy body (Fig. 4G). Some cells with perikarya and processes were filled with p-S129-α-syn-immunoreactive products (Fig. 4H and I). Fragmented p-S129-α-syn-immunoreactive neuropil threads (Fig. 4J and K) were observed in substantia nigra. Histochemical analysis verified that aggregated

Table 2 Summary results at 15 months: percentage change from baseline

	Left striatum SUVR, % change at:					Right striatum SUVR, % change at:				
Animal ID	**3 months**	**6 months**	**9 months**	**12 months**	**15 months**	**3 months**	**6 months**	**9 months**	**12 months**	**15 months**
CN 8172	−13.4	−21.7	+37.63	+30.47	+1.61	−24.2	−28.7	+20.72	+17.27	−5.53
CN 8408	−1.4	+98.4	+59.69	+50.76	+31.09	−4.7	+104.5	+63.88	+53.82	+36.12
CN 8409	−5.4	+66.6	+62.82	+120.37	NA	−7.7	+71.6	+71.62	+119.36	NA
CN 8410	+6.6	+51.8	+83.93	+68.92	NA	+4.9	+54.5	+73.29	+68.16	NA
CN 8411	+40.7	+43.0	+116.96	+106.24	NA	+28.9	+22.2	+107.12	+98.52	NA
CN 8412	−23.0	−29.9	+29.82	+57.00	+22.82	−30.9	−39.8	+9.13	+51.93	+18.81
CN 8413	+19.4	+86.4	+55.90	+105.30	NA	+16.5	−28.7	+39.82	+90.08	NA
CN 8414	+14.6	−17.9	+17.14	+51.10	+39.31	+18.4	+104.5	+23.35	+49.41	+38.92
CN 8415	−25.0	NA	NA	NA	NA	−28.0	NA	NA	NA	NA
Average	**1.45**	**34.58**	**57.98****	**73.77*****	**23.70**	**−2.97**	**32.51**	**51.11***	**68.56****	22.08

Occipital was used as a reference region.
(−) = reduction; (+) = increase; NA = not available; *$P < 0.05$, **$P < 0.01$, *** $P < 0.001$ as compared with baseline.

α-syn was thioflavin S-positive but cytoplasmic α-syn was not (Fig. 4L). There was undetectable p-S129-α-syn-immunoreactive product in amygdala as well as caudate nucleus. Some p-S129-α-syn-immunoreactive cells were observed in cortex near needle track (data not shown). Stereological analysis demonstrated that the number of p-S129-α-syn-immunoreactive cells was ∼800–8010 in substantia nigra (Table 1).

Reduction of TH-immunoreactivity in nigrostriatal system

The results above indicated that the injected α-syn PFFs in putamen were transported from the putamen to the substantia nigra and induced α-syn accumulation and aggregation in nigral neurons. We then tested whether α-syn aggregations induced by PFFs results in degeneration of nigral dopaminergic neurons. Stereological analyses demonstrated that there was a significant decrease of TH-immunoreactive neuronal number 29.3% reduction; (Fig. 5E) in ipsilateral but not contralateral substantia nigra as compared with controls [$F(2,18) = 6.12$; $P < 0.05$].

Qualitatively, some areas displayed much lighter TH immunostaining in the ipsilateral substantia nigra (Fig. 5C) than controls (Fig. 5A). Within this area, neurons had light TH staining with reduction of processes (Fig. 5D). We wanted to know whether decrease of TH expression was associated with p-S129-α-syn accumulation and aggregation induced by PFFs. Double immunostaining for TH and p-S129-α-syn was performed in nigral sections and co-localization analyses revealed that intense TH immunoreactivities were observed in the neurons without p-S129-α-syn inclusions while neurons with p-S129-α-syn inclusions had significantly lower TH immunoreactivities (Fig. 6A–C) in ipsilateral nigra compared with controls (Fig. 6D–F). To determine whether decreases in TH protein levels were associated with p-S129-α-syn inclusions, densitometer measurement (see 'Materials and methods' section) was performed on individual TH-immunoreactive neurons with present or absent p-S129-α-syn inclusions. An ANOVA revealed a significant difference in TH-immunoreactive intensities in nigral neurons [$F(3,11) = 72.78$; $P < 0.0001$]. *Post hoc* analyses revealed that relative to controls, there was a significant reduction of TH levels in the nigral neurons with p-S129-α-syn inclusions but not in the neurons with absent p-S129-α-syn (Fig. 6M).

Co-localization and quantitative analysis of p-S129-α-syn- and Nurr1-immunoreactivity in nigral neurons

Nurr1 is essential for the dopamine phenotype and the neuronal survival (Zetterstrom *et al.*, 1997; Chu *et al.*, 2006). Nurr1 expression is remarkably decreased in remaining nigral neurons in Parkinson's disease; specifically in neurons that express α-syn (Chu *et al.*, 2006). To determine whether a similar phenomenon occurred in the present model, we tested the hypothesis that the Nurr1 expression in nigral neurons was reduced by PFFs induced inclusions. To evaluate this possibility, we examined the co-localization of Nurr1 and p-S129-α-syn inclusions. Double labelling revealed that nigral neurons with p-S129-α-syn inclusions displayed significantly lower density of Nurr1 immunoreactivity but neurons without p-S129-α-syn inclusions exhibited intensive Nurr1 staining similar to controls (Fig. 6G–L). To determine whether decrease of in Nurr1 levels were associated with p-S129-α-syn inclusions, we analysed the relative intensities of Nurr1 immunofluorescence in nigral neurons that did or did not contain p-S129-α-syn inclusions. An ANOVA revealed a significant difference in the optical density of Nurr1 intensity among groups [$F(2,11) = 72.78$; $P < 0.0001$]. Interestingly, *post hoc* analyses revealed that, relative to controls, the optical density of Nurr1 immunofluorescent intensity was significantly decreased in nigral neurons with p-S129-α-syn

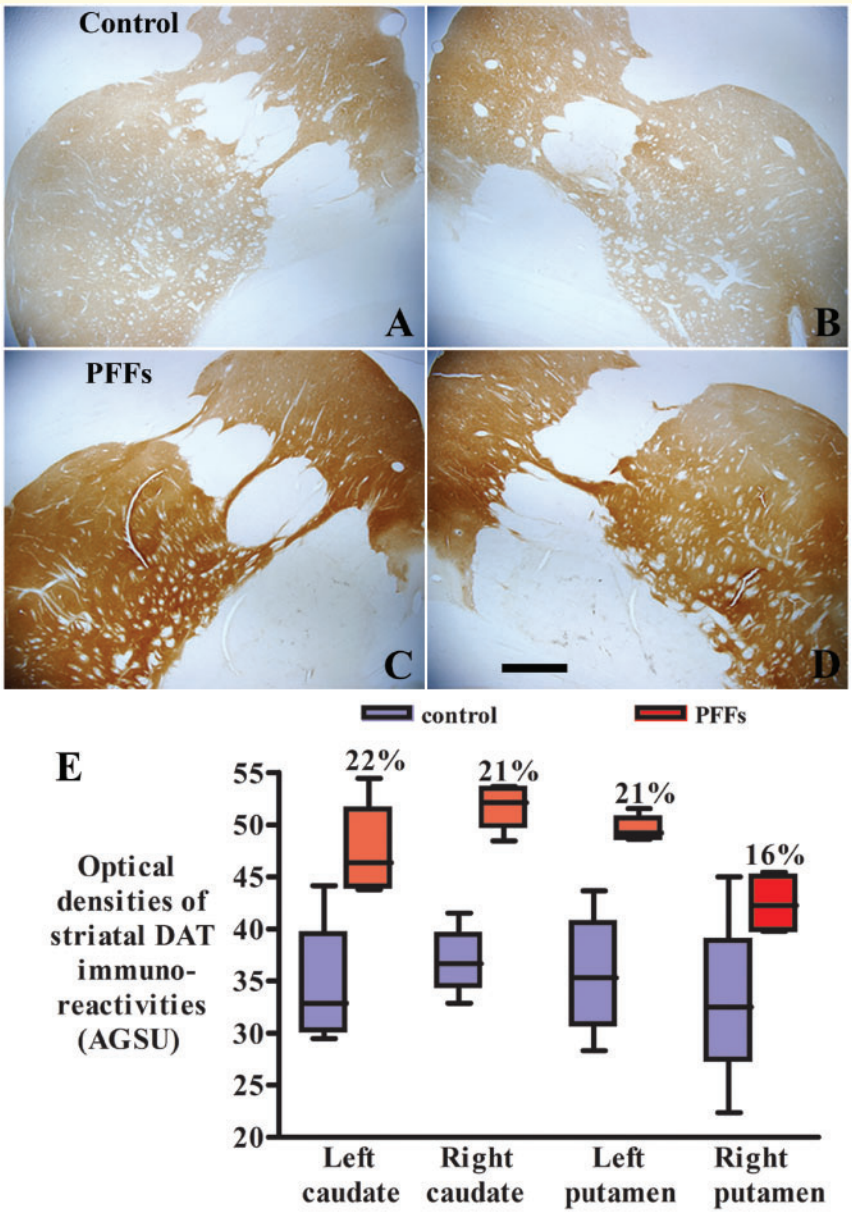

Figure 2 Microscopy images show DAT staining in monkeys receiving the sham surgery (control; A and B) and α-syn PFFs (C and D). The striatal DAT staining was light and homogenous in the monkey with sham surgery (**A** and **B**). Intensive DAT staining displayed in both caudate nuclei and putamen in monkeys receiving PFFs (**C** and **D**). Scale bar in **D** = 830 μm (applies to all). Quantitative optical density measurement (**E**) revealed further that the optical density of DAT staining was higher in striatum of monkeys receiving the α-syn PFFs than sham surgery (**E**; $P < 0.01$). AGSU = arbitrary greyscale units.

inclusions but not in neurons without p-S129-α-syn inclusions (Fig. 6N).

Co-localization and quantitative analysis of p-S129-α-syn- and DARPP-32-immunoreactivity in putamenal neurons

The delivery of PFFs into putamen induced p-S129-α-syn accumulations in striatal neurons around injection areas (Fig. 3). We tested whether the accumulated α-syn interfered with striatal neuronal function. To this end, coexistence of p-S129-α-syn and DARPP-32 was examined with immunofluorescent double-labelling. The neurons with p-S129-α-syn accumulation displayed reduction of DARPP-32-immunoreactivities while neurons with absent p-S129-α-syn accumulation had intense DARPP-32 immunostaining (Supplementary Fig. 3F). Densitometric measurement determined further that there was a significant reduction of DARPP-32 protein levels in the striatal neurons with present p-S129-α-syn accumulations but not in

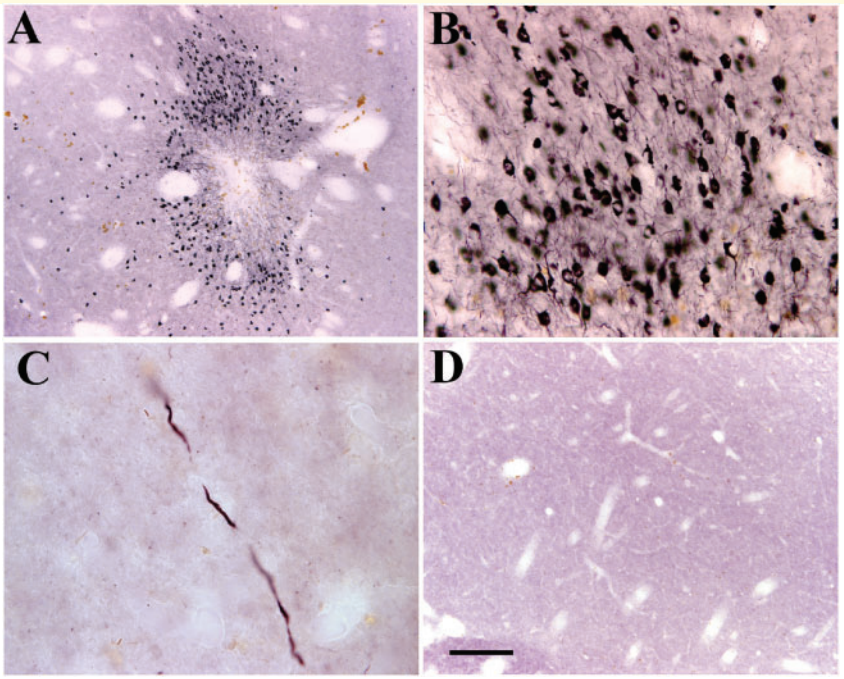

Figure 3 Sections from putamen show phosphorylated α-syn immunostaining in monkeys received α-syn PFFs (A–C) and sham surgery (D). The cells labelled with α-syn phosphorylated on Ser129 (p-S129-α-syn) were distributed around injected area (**A**) and displayed a strong dark immunostaining of α-syn (**B**). The p-S129-α-syn immuno-labelled fibres were detected far from injection area (**C**). There was an undetectable p-S129-α-syn in monkeys with sham surgery (**D**). Scale bar in **D** = 200 μm for **A**, 50 μm for **B**, and 20 μm for **C**.

the striatal neurons with absent p-S129-α-syn accumulation as compared with controls [$F(2,11) = 44.63$; $P < 0.0002$; Supplementary Fig. 3G].

Discussion

Here we demonstrate that α-syn PFFs, injected into the monkey putamen, cause Lewy pathology in nigral neurons and likely induce the recruitment of endogenous cytoplasm α-syn into pathological Lewy body- and Lewy neurite-like α-syn inclusions. Unfortunately there is no antibody to distinguish between monkey and human α-syn as they differ only by two amino acids and this point could not be confirmed empirically. Thioflavin S staining verified that α-syn PFFs templated α-syn inclusion is beta sheet-rich structures similar to Lewy body in Parkinson's disease brain. Nigral neurons with α-syn inclusions lost their TH and Nurr1 expressions as is seen in nigral neurons of human Parkinson's disease cases with α-syn aggregates (Chu *et al.*, 2006). About 29% of TH immunoreactive neuronal numbers were lost in ipsilateral substantia nigra compared with controls. DAT binding and DAT immunoreactive were increased after PFF injection possibly participating as part of an initial pathogenic process.

α-Syn PFFs can induce Lewy body pathology in neurons (Volpicelli-Daley *et al.*, 2014; Fares *et al.*, 2016; Tapias *et al.*, 2017; Panattoni *et al.*, 2018) in culture and in the rodent brain (Luk *et al.*, 2012; Paumier *et al* 2015; Karampetsou *et al.*, 2017). These studies have repeatedly verified that exogenous α-syn PFFs initiate pathological alterations in Parkinson's disease models. In our non-human primate model, α-syn inclusions displayed different shapes which might illustrate the processes of Lewy body formation. The α-syn granule-like seeds in nigral neurons may be transported from injected α-syn PFFs in putamen. The α-syn seeds serve as an initial 'template' that catalyses the conversion of resident normal α-syn into pathological micro-aggregates. All the while, the 'seeded' neuron produces more normal α-syn to compensate so that cytoplasmic α-syn can now be detected in nigral perikarya by immunohistochemistry. Excess levels of α-syn overwhelm the capacity of proteasomal and lysosomal systems to clear the protein (Chu *et al.*, 2009; Ghavami *et al.*, 2014). More and more α-syn micro-aggregates were replicated using seed templates and the cytoplasmic α-syn produced continually by neuron. Finally, the α-syn micro-aggregates filled the perikarya and main processes. When micro-aggregates form a mass like a Lewy body, the cell body and processes disappear. Thioflavin S staining further verified that the large Lewy body like α-syn aggregates was beta sheet-rich structures and not cytoplasmic α-syn. The pathological features we observed in monkey brain injected with PFFs are also detected in Parkinson's disease brain (Chu and Kordower, 2015) suggesting that PFFs induced a pathological process of α-syn seeding, accumulation, and aggregation similar to Parkinson's

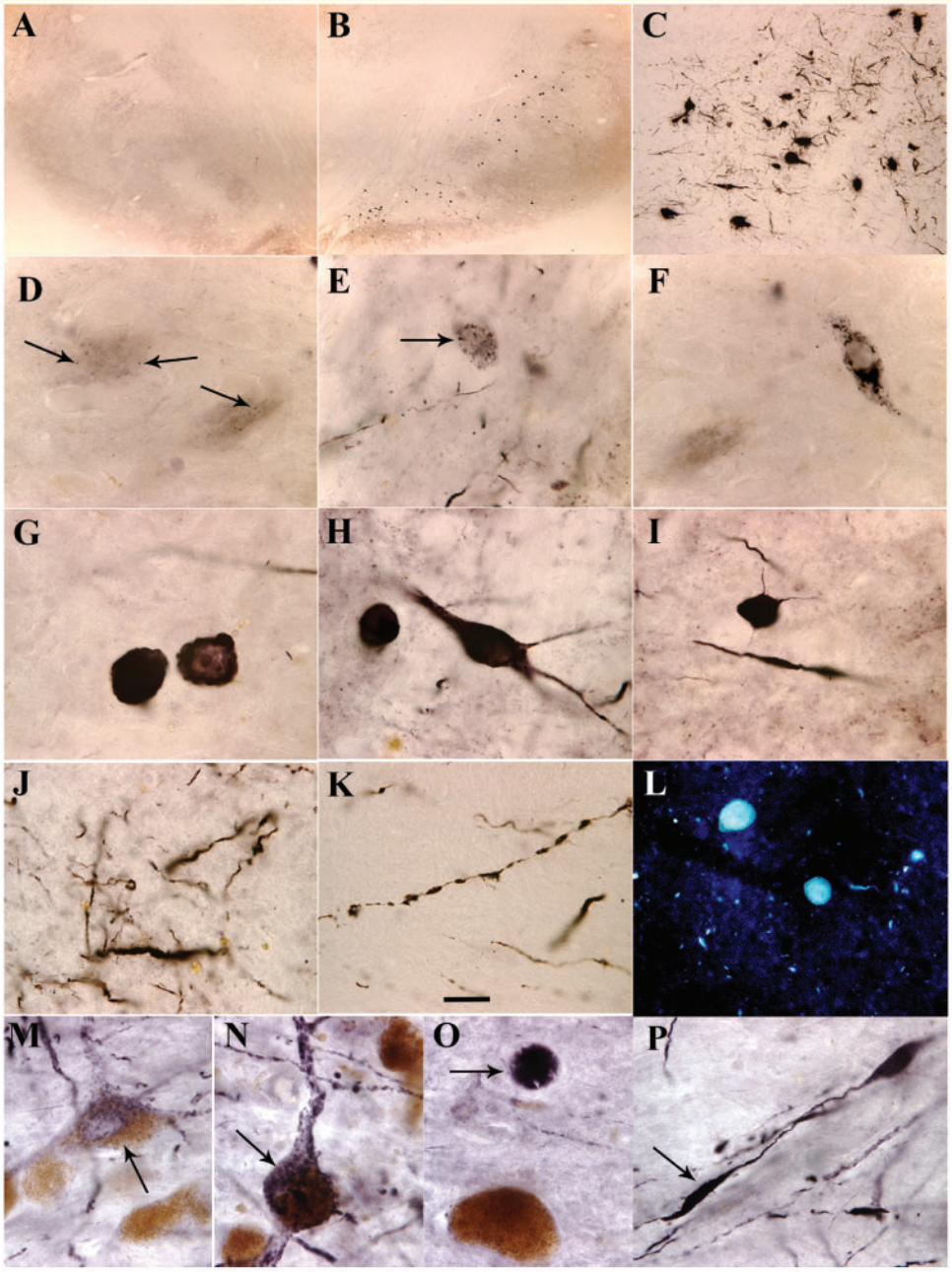

Figure 4 Microscopy images of substantia nigra. Shown are α-syn phosphorylated on Ser129 (p-S129-α-syn) immunoreactivity (**A**–**K** and **M**–**P**) and thioflavin S staining (**L**) from monkeys received α-syn PFFs (**B**–**L**), sham surgery (**A**) and patient with Parkinson's disease (**M**–**P**). Abundant p-S129-α-syn immunoreactive cells were distributed in substantia nigra pars compacta (**B** and **C**). These cells exhibited several morphological features: granules (arrows, **D**–**F**) with cytoplasmic staining, typical Lewy body with absent cytoplasm (**G**), and whole cells filled with p-S129-α-syn-immunoreactive products (**H** and **I**). Fragmental p-S129-α-syn-immunoreactive neuropil threads were observed in substantia nigra (**J** and **K**). Thioflavin S-positive inclusions were detected in substantia nigra (**L**). These pathological characteristics observed from monkeys received α-syn PFFs were similar to the Parkinson's disease; p-S129-α-syn immunoreactive products displayed granules (arrow, **M**), whole cell shape (arrow, **N**), Lewy body-like (arrow, **O**), and fragmental fibre (arrow, **P**). Scale bar in **K** = 20 μm and applies to **D**–**P**; 100 μm for **C**; and 500 μm for **A** and **B**.

disease. In this non-human primate model of Parkinson's disease, as well as human Parkinson's disease, the morphological characteristics of α-syn inclusions support the hypothesis that the pathological phenotypes are caused by 'seeded' corruption of endogenous α-syn likely through both a loss of normal α-syn function and gains of toxic functions from the accumulation of the Lewy Body-like inclusions, rather than exposure to the synthetic fibrils themselves (Kordower, 2014; Volpicelli-Daley *et al.*, 2014).

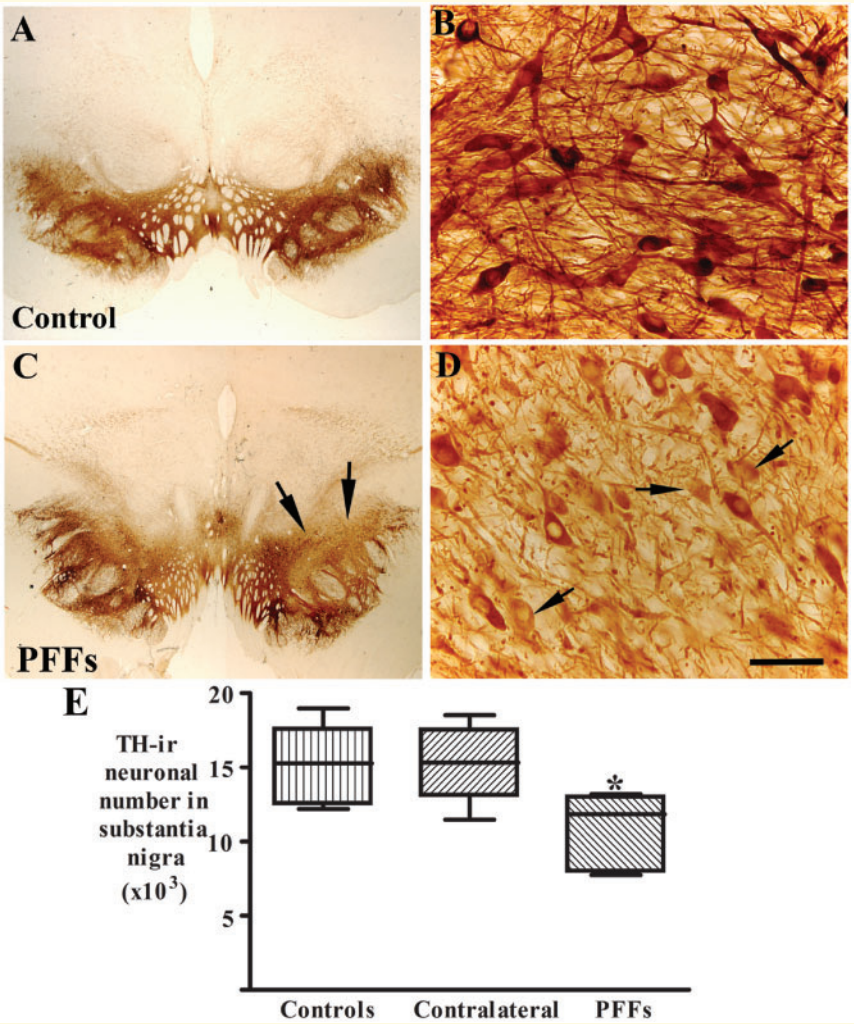

Figure 5 Patterns of TH immunoreactivities in substantia nigra from monkeys receiving sham surgery (control; A and B) and α-syn PFFs (C and D). There was a clear reduction of TH immunoreactivity in α-syn PFFs injected monkeys (arrows, **C**) compared with control monkeys (**A**). Some nigral neurons displayed light TH immunoreactivities with absent processes (arrows, **D**). Scale bar in **D** = 50 μm for **B** and 1.6 mm for **A** and **C**. (**E**) The number of TH-immunoreactive (-ir) neurons was reduced in the ipsilateral (PFFs, $^*P < 0.05$) but not contralateral ($P > 0.05$) substantia nigra as compared with controls. Data are mean ± standard deviation.

Both ^{123}I-PE2I SPECT imaging and immunohistochemical analyses revealed that DAT expression was increased in both ipsilateral and contralateral striatum after α-syn PFFs were delivered into unilateral putamen. SUVR was gradually increased from 3 months to 12 months followed by a decreasing binding at the 15-month time points suggesting that DAT activity is modulated by α-syn. The magnitude of these changes is enormous especially in light of injection of PFF's into an intact brain. The pattern and direction of these changes in DAT were confirmed by immunohistochemistry. Although these changes were not as robust using this procedure, the magnitude of optical density measurements are dependent upon a number of parameters not the least of which being the light intensity from the microscope. While the bilateral changes of DAT and changes seen in both caudate and putamen were surprising, the alterations in nigrostriatal function in striatal compartments anatomically unrelated to the injection site is not without precedent as injections of Lewy body extracts to the monkey putamen results in loss of dopamine markers in the caudate nuclei (Recasens *et al.*, 2014; see discussion in Kordower, 2014). These data are consistent with prior studies showing DAT compensation in following AAV-A53T rat model (Koprich *et al.*, 2011), midbrain dopaminergic cell model (Butler *et al.*, 2015), and more recent (unpublished) human data form the Parkinson Progression Marker Initiative (PPMI) showing an increase in DAT binding in unaffected LRRK2 and GBA mutation carriers prior to the onset of motor parkinsonism. Normally, DAT is a presynaptic membrane protein (McHugh and Buckley, 2015) essential for removing dopamine from the synaptic cleft, thus terminating dopamine signalling (Torres *et al.*, 2003). Although DAT is selective for its respective neurotransmitter dopamine

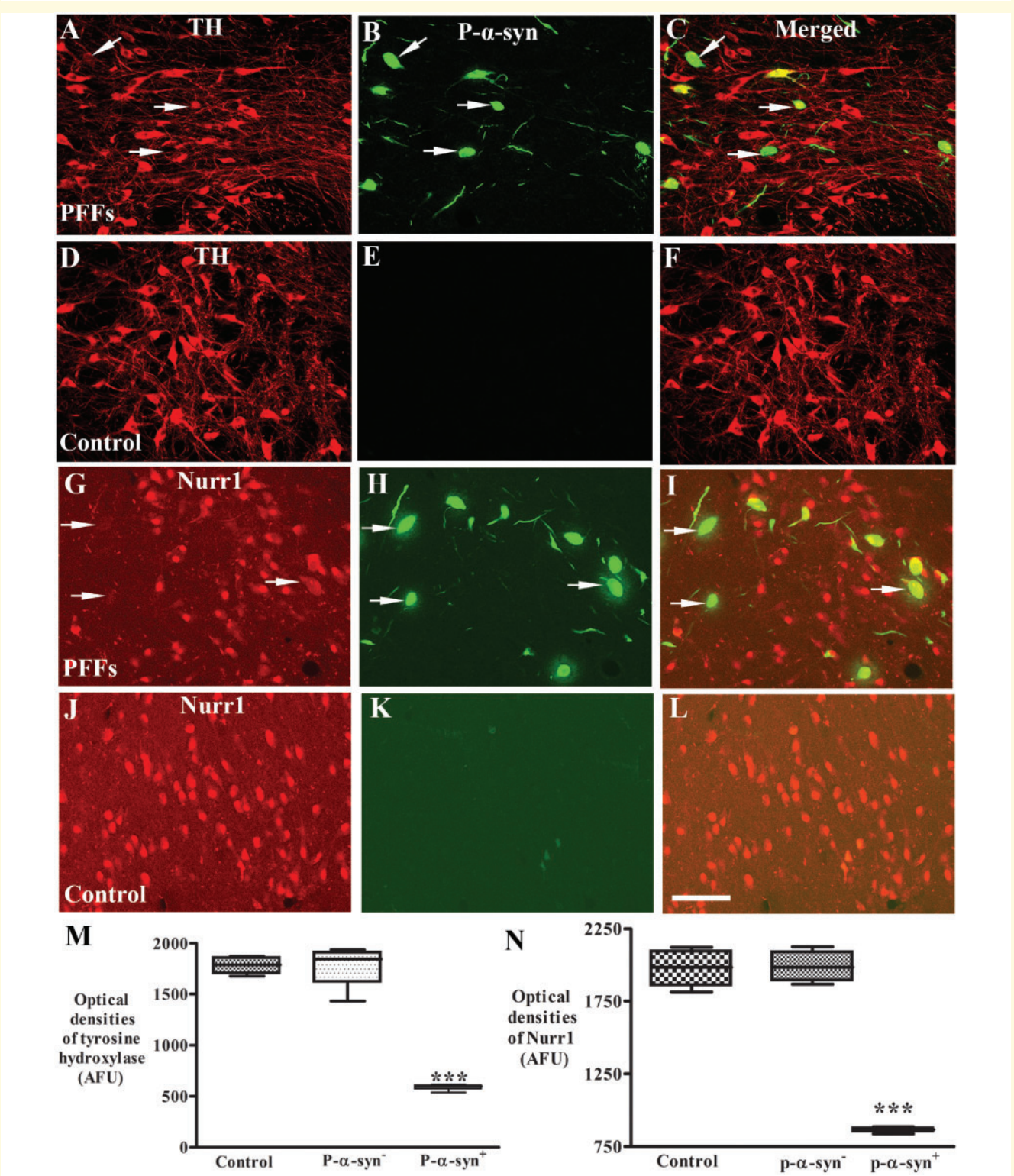

Figure 6 Laser confocal microscopic images of substantia nigra. Images are from monkeys receiving PFFs (**A**–**C** and **G**–**I**) and sham surgery (control; **D**–**F** and **J**–**L**) illustrating tyrosine hydroxylase (TH: red; **A** and **D**), Nurr1 (red; **G** and **J**), phosphorylated α-syn (P-α-syn: green; **B**, **E**, **H** and **K**), and the co-localization (merged; **C**, **F**, **I** and **L**). Note that TH immunofluorescence intensity was severely diminished (arrows; **A** and **C**) in the neurons with p-S129-α-syn (arrows; **B** and **C**) immunoreactive inclusions but not in neurons without P-α-syn-immunoreactive inclusions in monkeys received α-syn PFFs. Similarly, Nurr1 immunofluorescence intensity was severely diminished in the neurons (arrows; **G** and **I**) with p-α-syn immunoreactive inclusions (arrows; **H** and **I**) but not in neurons without P-α-syn immunoreactive inclusions. In contrast, no P-α-syn immunoreactive inclusions were observed in monkeys with sham surgery (**E** and **K**). Scale bar in **L** = 110 μm (applies to all). Quantitative measurement further revealed that the optic densities of TH (**M**) and Nurr1 (**N**) were significantly decreased in the neurons with P-α-syn immunopositive (P-α-syn^{+}) but not in neurons with P-α-syn immunonegative (P-α-syn^{-}) inclusion as compared with monkeys with sham surgery. $^{***}P < 0.001$, compared with sham surgery. AFU = arbitrary fluorescence units.

(Storch *et al.*, 2004), it also binds α-syn (Lee *et al.*, 2001) and neurotoxins (Nass and Blakely, 2003; Swant *et al.*, 2011). Several studies have reported that DAT interacts with α-syn to regulate its activity and its membrane distribution (Sidhu *et al.*, 2004; Bellucci *et al.*, 2011; Butler *et al.*, 2015; Bridi and Hirth, 2018). Study of the yeast two-hybrid system has demonstrated that α-syn directly interacts with DAT and accelerates dopamine-induced apoptosis (Lee *et al.*, 2001). Double staining revealed that DAT-labelled striatal fibres and terminals coexisted with α-syn suggesting that the DAT is associated with the pathological species converted by exogenous α-syn PFFs. Using an *in situ* proximity ligation assay, DAT/α-syn interactions can be detected in striatum of Parkinson's disease (Longhena *et al.*, 2018). This suggests that the DAT/α-syn complex could lose its function to pump dopamine from synaptic cleft back into cytosol (Sidhu *et al.*, 2004) instead of translocation of α-syn from plasma membrane to cytoplasm (Bellucci *et al.*, 2011).

The mechanism of increasing DAT expression by α-syn PFFs delivery into putamen is unknown. The overexpression of α-syn protein can increase the number of DAT binding sites in the caudate and putamen in cocaine users compared with age-matched drug-free controls (Gelernter *et al.*, 1994; Qin *et al.*, 2005). Whether DAT overexpression detected in this study reflects binding to exogenous α-syn PFFs or whether DAT/α-syn complex results in DAT overexpression will require additional studies. Nonetheless, the DAT overexpression may be an important part of the initial and degenerative process or may be compensatory for offsetting elevated levels of synaptic dopamine. The DAT/α-syn PFFs complex may allow pathological α-syn fibrils to invade dopaminergic terminals and to be retrogradely transported to cell body in substantia nigra. It may explain that α-syn inclusions were mainly detected in substantia nigra after α-syn PFFs were delivered to monkey putamen. More studies are needed to determine pathological effects of α-syn /DAT complex on Parkinson's disease.

Nurr1 plays a key role in the maintenance and survival of the dopaminergic system (Jankovic *et al.*, 2005; Sacchetti *et al.*, 2006; Dong *et al.*, 2016). Genetic deletion of Nurr1 in mice can cause the absence of dopaminergic neurons in the substantia nigra and ventral tegmental area (Zetterstrom *et al.*, 1997). Our previous study revealed that the levels of Nurr1 were positively correlated with TH expression in nigral dopaminergic neurons (Chu *et al.*, 2006). In the Parkinson's disease brain, both TH and Nurr1 expression are markedly reduced in nigral neurons with α-syn inclusions but not the neurons without α-syn inclusions. Almost identical results were seen in the present study in monkeys receiving α-syn PFFs. Indeed, nigral neurons with α-syn inclusions displayed significant reductions of TH and Nurr1 whereas neurons without α-syn inclusions exhibited intense TH and Nurr1 expression. It is clear that Nurr1, a transcriptional factor, regulates several genes involved in the dopamine neuronal functions, ranging from the dopamine metabolism, neurotransmission, axonal growth, mitochondrial function and cell survival (Decressac *et al.*, 2012; Heng *et al.*, 2012; Kadkhodaei *et al.*, 2013), Dopaminergic neuronal survival is associated with glial cell line-derived neurotrophic factor (GDNF) and it's receptor, the proto-oncogene tyrosine-protein kinase receptor Ret (Ayanlaja *et al.*, 2018). Ret is regulated by Nurr1 (Wallén *et al.*, 2001; Galleguillos *et al.*, 2010). The accumulation of α-syn may interrupt the function of Nurr1 through the direct or indirect interference with the signalling of GDNF receptor Ret and result in GDNF fail to exert neuroprotective effect in Parkinson's disease (Decressac *et al.*, 2013). Our findings provide an insight understanding that reduced Nurr1 expression may predispose dopaminergic neurons toward a cascade that begins with a phenotypic downregulation of dopaminergic tone to events ultimately leading to their demise.

Striatal neuritic pathology has also been described in prodromal Parkinson's disease (Chu *et al.*, 2018) and some familial Parkinson's disease patients bearing mutations or multiplication *SNCA* (Kotzbauer *et al.*, 2004; Yamaguchi *et al.*, 2005). Neuronal α-syn inclusions (Mori *et al.*, 2008) and neuronal loss (Bugiani *et al.*, 1980) in the neostriatum had been found in Parkinson's disease. Our data demonstrated that exogenous α-syn PFFs induced α-syn accumulation in striatal neurons and caused neurodegeneration similar to that seen pathologically in Parkinson's disease (Bugiani *et al.*, 1980). These finding suggest that the striatal neurons degenerate through α-syn accumulation and aggregation during Parkinson's disease progression. As the striatum is located in the centre of the brain and connected widely to brain areas, the striatal α-syn inclusions are the pathogens that persistently propagate pathological α-syn seeds to different brain areas including substantia nigra. Some p-α-syn-immunopositive cells were observed in cortex. Whether the cortical p-α-syn accumulation and aggregation were associated with putamenal or needle track PFF delivery requires further examination.

In summary, the present data indicate that exogenous α-syn PFFs are internalized by dopaminergic terminals, spread to nigra, and induce Parkinson's disease-like pathology including α-syn aggregation and nigral neuronal degeneration. α-syn PFFs induced DAT expression possibly to compensate for reduction in dopaminergic nerve terminal function. The DAT/α-syn PFF complex formation may initiate Parkinson's disease pathology in dopaminergic neurons. The pathological effects of DAT/α-syn should be investigated in Parkinson's disease brain.

Funding

This study was supported by a grant from the Michael J. Fox Foundation.

Competing interests

The authors report no competing interests.

Supplementary material

Supplementary material is available at *Brain* online.

References

Ayanlaja AA, Zhang B, Ji G, Gao Y, Wang J, Kanwore K, Gao D. The reversible effects of glial cell line-derived neurotrophic factor (GDNF) in the human brain. Semin Cancer Biol 2018; 53: 212–22.

Bellucci A, Navarria L, Falarti E, Zaltieri M, Bono F, Collo G, et al. Redistribution of DAT/α-synuclein complexes visualized by "in situ" proximity ligation assay in transgenic mice modelling early Parkinson's disease. PLoS One 2011; 6: 1–12.

Bridi JC, Hirth F. Mechanisms of α-Synuclein induced synaptopathy in Parkinson's disease. Front Neurosci 2018; 12: 1–20.

Bugiani O, Perdelli F, Salvarani S, Leonardi A, Mancardi GL. Loss of striatal neurons in Parkinson's disease a cytometric study. Eur Neurol 1980; 19: 339–44.

Butler B, Saha K, Rana T, Becker JP, Sambo D, Davari P, et al. Dopamine transporter activity is modulated by α-Synuclein. J Biol Chem 2015; 290: 29542–54.

Chang T, Diab RH, Clark JW Jr, Mawlawi OR. Investigating the use of nonattenuation corrected PET images for the attenuation correction of PET data. Med Phys 2013; 40: 082508–13.

Chu Y, Buchman AS, Olanow CW, Kordower JH. Do subjects with minimal motor features have prodromal Parkinson disease? Ann Neurol 2018; 83: 562–74.

Chu Y, Dodiya H, Aebischer P, Olanow CW, Kordower JH. Alterations in lysosomal and proteasomal markers in Parkinson's disease: relationship to alpha-synuclein inclusions. Neurobiol Dis 2009; 35: 385–98.

Chu Y, Goldman JG, Kelly L, He Y, Waliczek T, Kordower JH. Abnormal alpha-synuclein reduces nigral voltage-dependent anion channel 1 in sporadic and experimental Parkinson's disease. Neurobiol Dis 2014; 69:1–14.

Chu Y, Kordower JH. Age-associated increases of alpha-synuclein in monkeys and humans are associated with nigrostriatal dopamine depletion: is this the target for Parkinson's disease? Neurobiol Dis 2007; 25: 134–49.

Chu Y, Kordower JH. Lewy body pathology in fetal grafts. Ann N Y Acad Sci 2010; 1184: 55–67.

Chu Y, Kordower JH. The prion hypothesis of Parkinson's disease. Curr Neurol Neurosci Rep 2015; 15: 28: 1–10.

Chu Y, Le W, Kompoliti K, Jankovic J, Mufson EJ, Kordower JH. Nurr1 in Parkinson's disease and related disorders. J Comp Neurol 2006; 494: 495–514.

Chu Y, Morfini GA, Langhamer LB, He Y, Brady ST, Kordower JH. Alterations in axonal transport motor proteins in sporadic and experimental Parkinson's disease. Brain 2012; 135: 2058–73.

Collier TJ, Lipton J, Daley BF, Palfi S, Chu Y, Sortwell C, et al. Aging-related changes in the nigrostriatal dopamine system and the response to MPTP in nonhuman primates: diminished compensatory mechanisms as a prelude to Parkinsonism. Neurobiol Dis 2007; 26: 56–65.

Dawson T, Mandir A, Lee M. Animal models of PD: pieces of the same puzzle? Neuron 2002; 35: 219–22.

Decressac M, Kadkhodaei B, Mattsson B, Laguna A, Perlmann T, Bjorklund A. α-Synuclein-induced down-regulation of Nurr1 disrupts GDNF signaling in nigral dopamine neurons. Sci Transl Med 2012; 4: 163ra156.

Decressac M, Volakakis N, Björklund A, Perlmann T. NURR1 in Parkinson disease–from pathogenesis to therapeutic potential. Nat Rev Neurol 2013; 9: 629–36.

Dong J, Li S, Mo JL, Cai HB, Le WD. Nurr1-based therapies for Parkinson's Disease. CNS Neurosci Ther 2016; 22: 351–9.

Fares MB, Maco B, Oueslati A, Rockenstein E, Ninkina N, Buchman VL, et al. Induction of de novo α-synuclein fibrillization in a neuronal model for Parkinson's disease. Proc Natl Acad Sci USA 2016; 113: E912–21.

Froula JM, Henderson BW, Gonzalez JC, Vaden JH, Mclean JW, Wu Y, et al. α-Synuclein fibril-induced paradoxical structural and functional defects in hippocampal neurons. Acta Neuropathol. Commun 2018; 6: 1–13.

Galleguillos D, Fuentealba JA, Gómez LM, Saver M, Gómez A, Nash K, et al. Nurr1 regulates RET expression in dopamine neurons of adult rat midbrain. J Neurochem 2010;114: 1158–67.

Gelernter J, Kranzler HR, Satel SL, Rao PA. Genetic association between dopamine transporter protein alleles and cocaine-induced paranoia. Neuropsychopharmacology 1994; 11: 195–200.

Ghavami S, Shojaei S, Yeganeh B, Ande SR, Jangamreddy JR, Mehrpour M, et al. Autophagy and apoptosis dysfunction in neurodegenerative disorders. Prog Neurobiol 2014; 112: 24–49.

Gundersen HJ, Bendtsen TF, Korbo L, Marcussen N, Møller A, Nielsen K, et al. Some new, simple and efficient stereological methods and their use in pathological research and diagnosis. APMIS 1988; 96: 379–94.

Heng X, Jin G, Zhang X, Yang D, Zhu M, Fu S, et al. Nurr1 regulates Top IIß and functions in axon genesis of mesencephalic dopaminergic neurons. Mol Neurodegener 2012; 7: 4.

Irwin RP, Nutt JG, Woodward WR, Gancher ST. 1992. Pharmacodynamics of the hypotensive effect of levodopa in parkinsonian patients. Clin Neuropharmacol 1992; 15: 365–74.

Jankovic J, Chen S, Le WD. The role of Nurr1 in the development of dopaminergic neurons and Parkinson's disease. Prog Neurobiol 2005; 77: 128–38.

Kadkhodaei B, Alvarsson A, Schintu N, Ramsköld D, Volakakis N, Joodmardi E, et al. Transcription factor Nurr1 maintains fiber integrity and nuclear-encoded mitochondrial gene expression in dopamine neurons. Proc Natl Acad Sci USA 2013; 110: 2360–5.

Kanaan NM, Kordower JH, Collier TJ. Age-related accumulation of Marinesco bodies and lipofuscin in rhesus monkey midbrain dopamine neurons: relevance to selective neuronal vulnerability. J Comp Neurol 2007; 502: 683–700.

Karampetsou M, Ardah MT, Semitekolou M, Polissidis A, Samiotaki M, Kalomoiri M, et al. Phosphorylated exogenous alpha-synuclein fibrils exacerbate pathology and induce neuronal dysfunction in mice. Sci Rep 2017; 7: 16533.

Kellie JF, Higgs RE, Ryder JW, Major A, Beach TG, Adler CH, et al. Quantitative measurement of intact alpha-synuclein proteoforms from post-mortem control and Parkinson's disease brain tissue by intact protein mass spectrometry. Sci. Rep 2014; 4: 1–10.

Koprich JB, Johnston TH, Huot P, Reyes MG, Espinosa M, Brotchie JM. Progressive neurodegeneration or endogenous compensation in an animal model of Parkinson's disease produced by decreasing doses of alpha-synuclein. PLoS One 2011; 6: 1–9.

Kordower JH. The prion hypothesis of Parkinson's disease: this hot topic just got hotter. Mov Disord 2014; 29: 988

Kordower JH, Brundin P. Propagation of host disease to grafted neurons: accumulating evidence. Exp Neurol 2009; 220: 224–5.

Kordower JH, Chu Y, Hauser RA, Freeman TB, Olanow CW. Lewy body-like pathology in long-term embryonic nigral transplants in Parkinson's disease. Nat Med 2008; 14: 504–6.

Kordower JH, Goetz CG, Chu Y, Halliday GM, Nicholson DA, Musial TF, et al. Robust graft survival and normalized dopaminergic innervation do not obligate recovery in a Parkinson disease patient. Ann Neurol 2017; 81: 46–57.

Kotzbauer PT, Giasson BI, Kravitz AV, Golbe LI, Mark MH, Trojanowski JQ, et al. Fibrillization of α-synuclein and tauin

familial Parkinson's disease caused by the A53T α-synuclein mutation. Exp Neurol 2004; 187: 279–88.

Lee FJ, Liu F, Pristupa ZB, Niznik HB. Direct binding and functional coupling of alpha-synuclein to the dopamine transporters accelerate dopamine-induced apoptosis. FASEB J 2001; 15: 916–26.

Li JY, Englund E, Holton JL, Soulet D, Hagell P, Lees AJ, et al. Lewy bodies in grafted neurons in subjects with Parkinson's disease suggest host-to-graft disease propagation. Nat Med 2008; 14: 501–3.

Longhena F, Faustini G, Missale C, Pizzi M, Bellucci A. Dopamine transporter/α-Synuclein complexes are altered in the post mortem caudate putamen of Parkinson's disease: an in situ proximity ligation assay study. Int J Mol Sci 2018; 19: 1–14.

Luk KC, Covell DJ, Kehm VM, Zhang B, Song IY, Byrne MD, et al. 2016. Molecular and biological compatibility with host alpha-synuclein influences fibril pathogenicity. Cell Rep 2016; 16: 3373–87.

Luk KC, Kehm V, Carroll J, Zhang B, O'Brien P, Trojanowski JQ, Lee VM. Pathological α-synuclein transmission initiates Parkinson-like neurodegeneration in nontransgenic mice. Science 2012; 338: 949–53.

McHugh PC, Buckley DA. The structure and function of the dopamine transporter and its role in CNS diseases. Vitam Horm 2015: 98: 339–69.

McNeill TH, Koek LL. Differential effects of advancing age on neurotransmitter cell loss in the substantia nigra and striatum of C57BL/6N mice. Brain Res 1990; 521: 107–117.

Miller GW, Staley JK, Heilman CJ, Perez JT, Mash DC, Rye DB, et al. Immunochemical analysis of dopamine transporter protein in Parkinson's disease. Ann Neurol 1997; 41: 530–9.

Moeller and Dimitrijevich. A new strategy for analysis of phenotype marker antigens in hollow neurospheres. J Neurosci Methods 2004; 139: 43–50.

Mori F, Tanji K, Zhang H, Kakita A, Takahashi H, Wakabayashi K. alpha-Synuclein pathology in the neostriatum in Parkinson's disease. Acta Neuropathol 2008; 115: 453–59.

Nass R, Blakely RD. The Caenorhabditis elegans dopaminergic system: opportunities for insights into dopamine transport and neurodegeneration. Annu Rev Pharmacol Toxicol 2003; 43: 521–44.

Panattoni G, Rota L, Colla E. Exogenous administration of microsomes-associated alpha-synuclein aggregates to primary neurons as a powerful cell model of fibrils formation. J Vis Exp 2018; 136: 1–9.

Pasinetti GM, Osterburg HH, Kelly AB, et al. Slow changes of tyrosine hydroxylase gene expression in dopaminergic brain neurons after neurotoxin lesioning: A model for neuron aging. Mol Brain Res 1992; 13: 63–73.

Paumier KL, Luk KC, Manfredsson FP, Kanaan NM, Lipton JW, Collier TJ, et al. 2015. Intrastriatal injection of pre-formed mouse α-synuclein fibrils into rats triggers α-synuclein pathology and bilateral nigrostriatal degeneration. Neurobiol Dis 2015; 82: 185–99.

Qin Y, Ouyang Q, Pablo J, Mash DC. 2005. Cocaine abuse elevates alpha-synuclein and dopamine transporter levels in the human striatum. Neuroreport 2005; 16: 1489–93.

Recasens A, Dehay B, Bové J, Carballo-Carbajal I, Dovero S, Pérez-Villalba A, et al. Lewy body extracts from Parkinson disease brains trigger α-synuclein pathology and neurodegeneration in mice and monkeys. Ann Neurol 2014; 75: 351–62.

Sacchetti P, Carpentier R, Ségard P, Olivé-Cren C, Lefebvre P. Multiple signaling pathways regulate the transcriptional activity of the orphan nuclear receptor NURR1. Nucleic Acids Res 2006; 34: 5515–27.

Sidhu A, Wersinger C, Vernier P. alpha-Synuclein regulation of the dopaminergic transporter: a possible role in the pathogenesis of Parkinson's disease. FEBS Lett 2004; 565: 1–5.

Steiner JA, Angot E, Brundin P. A deadly spread: cellular mechanisms of α-synuclein transfer. Cell Death Differ 2011; 18: 1425–33.

Storch A, Hwang YI, Gearhart DA, Beach JW, Neafsey EJ, Collins MA, et al. Dopamine transporter-mediated cytotoxicity of beta-carbolinium derivatives related to Parkinson's disease relationship to transporter-dependent uptake. J Neurochem 2004; 89: 685–94.

Swant J, Goodwin JS, North A, Ali AA, Gamble-George J, Chirwa S, Khoshbouei H. α-Synuclein stimulates a dopamine transporter-dependent chloride current and modulates the activity of the transporter. J Biol Chem 2011; 286: 43933–43.

Tapias V, Hu X, Luk KC, Sanders LH, Lee VM, Greenamyre JT. Synthetic alpha-synuclein fibrils cause mitochondrial impairment and selective dopamine neurodegeneration in part via iNOS-mediated nitric oxide production. Cell Mol Life Sci 2017; 74: 2851–74.

Tavares AA, Batis J, Barret O, Alagille D, Vala C, Kudej G, et al. In vivo evaluation of [(123)I]MNI-420 a novel single photon emission computed tomography radiotracer for imaging of adenosine 2A receptors in brain. Nucl Med Biol 2013; 40: 403–9.

Thakur P, Breger LS, Lundblad M, Wan OW, Mattsson B, Luk KC, et al. Modeling Parkinson's disease pathology by combination of fibril seeds and α-synuclein overexpression in the rat brain. Proc Natl Acad Sci U S A 2017; 114: E8284–93.

Torres GE, Carneiro A, Seamans K, Fiorentini C, Sweeney A, Yao WD, Caron MG. Oligomerization and trafficking of the human dopamine transporter. Mutational analysis identifies critical domains important for the functional expression of the transporter. J Biol Chem 2003; 278: 2731–9.

Volpicelli-Daley LA, Luk KC, Lee VM. Addition of exogenous α-synuclein preformed fibrils to primary neuronal cultures to seed recruitment of endogenous α-synuclein to Lewy body and Lewy neurite-like aggregates. Nat Protoc 2014; 9: 2135–46.

Volpicelli-Daley LA, Luk KC, Patel TP, Tanik SA, Riddle DM, Stieber A, et al. Exogenous α-synuclein fibrils induce Lewy body pathology leading to synaptic dysfunction and neuron death. Neuron 2011; 72: 57–71.

Wallén A A, Castro DS, Zetterström RH, Karlén M, Olson L, Ericson J, Perlmann T. Orphan nuclear receptor Nurr1 is essential for Ret expression in midbrain dopamine neurons and in the brain stem. Mol Cell Neurosci 2001; 18: 649–63.

Wiemerslage L, Schultz BJ, Ganguly A, Lee D. 2013. Selective degeneration of dopaminergic neurons by MPP(+) and its rescue by D2 autoreceptors in Drosophila primary culture. J Neurochem 2013; 126: 529–40.

Yamaguchi K, Cochran EJ, Murrell JR, Polymeropoulos MH, Shannon KM, Crowther RA, et al. Abundant neuritic inclusions and microvacuolar changes in a case of diffuse Lewy body disease with the A53T mutation in the α-synuclein gene. Acta Neuropathol 2005; 110: 298–305.

Zetterstrom RH, Solomin L, Jansson L, Hoffer BJ, Olson L, Perlmann T. Dopamine neuron agenesis in Nurr1-deficient mice. Science 1997; 276: 248–50.